Computations for Large Amplitude Two-Dimensional Body Motions

Xinshu Zhang and Robert F. Beck *
Department of Naval Architecture and Marine Engineering
University of Michigan, Ann Arbor, MI 48109

Abstract

A numerical method is presented for the time-domain simulation of large amplitude motions of a 2-D surface piercing body with arbitrary shape in deep water. Based on potential theory, panels are distributed on the body and desingularized sources are distributed above the calm water surface. The body boundary condition is satisfied on the exact submerged body surface. The free surface boundary conditions are linearized and satisfied on the calm water level. The solution is stepped forward in time by integrating the free surface kinematic and dynamic conditions. The numerical solutions for the oscillation problem are compared with experimental results and other numerical results, and found to agree well. The results for the impact problem are compared with similarity solutions. Finally, results for the large amplitude sinusoidal motion of a 45-degree wedge are presented.

1 Introduction

The accurate prediction of the wave-induced motions and loads is very important in ship and offshore design. Severe motions and extreme loads can lead to operability problems and in extreme cases structural failure and capsize. In the traditional approach to seakeeping calculations potential flow is assumed. The problem is linearized by assuming that the motions are small. The body boundary conditions are satisfied on the mean body surface and the free surface conditions are linearized about the calm water level. The problem can be solved in either the time domain or the frequency domain because in linear potential flow theory they are directly related by Fourier transforms. Linear system theory and random process theory is then used to predict the extreme responses and loads. The primary objection to the linear systems approach is that it often misses important features of extreme responses. For example, linear theory predicts that the hogging and sagging bending moments acting on a ship in a seaway have the same amplitude. In fact, due to nonlinearities, the hogging and sagging bending moments are significantly different. Another example is that linear theory (constant potential on the free surface) predicts that the vertical forces acting on a body entering or leaving the free surface have the same magnitude.

There are many variations to this linear approach. Strip theory (see Salvesen et al. [1]) is probably the most popular for long, slender ships. In this frequency domain approach, the solution to the three-dimensional problem is approximated by solving a series of two-dimensional problems in the cross-flow plane. The two-dimensional problem is usually solved using a boundary element method such as the one developed by Frank [2]. Frank's method uses constant source strength flat panels distributed over the mean submerged body contour. For offshore structures and more advance ship motion theories, 'panel methods' have been developed in which the mean wetted surface of the body is divided into panels and Green functions are used to solve the boundary value problem. The free surface may or may not be panelized depending on whether a Rankine source Green function or a free surface Green function is used. For example, Prof. Newman [3] and his students have used the zero-speed free-surface Green function and higher order panel methods to develop WAMIT, a code widely used in the offshore industry. A complete history of the various methods can be found in Beck and Reed [4].

The other extreme from linear theory is to retain potential flow, but solve the fully nonlinear problem. In this case the body boundary condition is satisfied on the exact wetted surface of the body and the fully nonlinear free surface boundary conditions are used. The computations are carried out in the time domain. The most common solution method is the mixed Euler-Lagrange, or MEL, method originally developed by Longuet-Higgins and Cokelet [5]. In this method, a linear mixed boundary value problem is solved at each time step with the potential given on the exact free surface and the normal velocity is prescribed on the exact wetted surface of the body. The nonlinear free surface boundary conditions are used to time step the potential on the free surface and the free-surface amplitude. The body boundary condition is either known for forced

*Corresponding author. rbeck@umich.edu; Ph.:(734) 764-0282

motions or is determined by solving the dynamic equations of motion for the body. Many results are available in both two and three dimensions (see for example Beck [6]). The problems with MEL computations are the instabilities of the free surface and wave breaking. The instabilities can often be eliminated by improved numerical techniques, but wave breaking is a natural phenomenon that is expected to occur in any large motion or wave situation. Computations normally are forced to stop when wave breaking occurs. Various techniques have been proposed to continue the computations after wave breaking, but they are not robust and can lead to nonphysical solutions.

A compromise between fully nonlinear computations and linear theory is the so-called double-body approach (see for example Sclavounos [7]). In this approach, the double-body flow is used to linearize the free surface boundary conditions on a known surface (usually the calm water level, but it can be the incident wave surface). The body boundary conditions can be solved on either the mean wetted surface or the exact position. Wave breaking is no longer a difficulty because the free surface boundary conditions are satisfied on a known surface. However, since free surface Green functions no longer meet the free surface boundary conditions, Rankine sources must be used and panels are distributed over both the body surface and the free surface. This in turn leads to difficulties on the edges of the computational domain and a large matrix inversion at each time step. The methods have shown improved seakeeping predictions, but computational costs preclude the method being used in preliminary design and optimization.

In order to develop computationally fast seakeeping calculations, but still retaining the important nonlinearities, blended methods in the time domain have been developed by several researchers (see for example the ISSC report [8], and Finn *et al.* [9]). Blended methods are a blend of linear and nonlinear approaches that have little rational basis. It is an engineering solution that combines the nonlinearities that are easily computed (the rigid body equations of motion, the nonlinear hydrostatic force and the Froude-Krylov exciting force) with linear hydrodynamic computations for the radiation and diffraction forces. Typically, blended methods use linear theory to compute the radiation and diffraction forces acting on a two-dimensional section of the ship. Strip theory approximations are then used to determine the three-dimensional hydrodynamic forces. To improve the validity of blended method computations and still retain the high computational speeds that are necessary, we have developed a body exact technique. In this approach, the two-dimensional boundary value problem is solved using an exact body boundary condition and a linearized free surface boundary condition satisfied on the calm water surface. Similar to the fully nonlinear MEL computations, at any time step the normal velocity is known on the exact body surface and the potential is given on the calm water level. The solution is time stepped using the known motions of the body and the linear free surface conditions. As will be shown, the advantages of the method are that it introduces the nonlinearities associated with the change in wetted surface of the body, while retaining the computational efficiency of the linearized free surface conditions. In addition, there are no breaking wave problems and numerical instabilities are minimized.

Another advantage of the present method is that it can deal easily with the water entry and exit problems, a situation that often exists in the bow and stern regions of high speed ships. The high pressures and impulse loads that occur during impact often set the structural design limits. Consequently, it is important that a blended method is able to access rapidly these types of loads. The first classic work on the impact problem was due to Von Karman [10] who developed an asymptotic theory for the near-flat impact using a linearized body boundary condition and a constant potential free surface condition. Wagner [11] went a step beyond Von Karman's solution by considering the effect of the water splash. Dobroboskaya [12] derived a similarity solution by using the geometric speciality of the body. The solution is valid only for small deadrise angles, and such a similarity solution does not exist for arbitrary bodies. Recently, Zhao and Faltinsen [13] used fully nonlinear free surface simulations to predict the slamming loads. This fully nonlinear method includes the spray roots that are developed at the intersection of the body and free surface. However, it can not be used for a long time simulation due to wave breaking. It should be noted that the body-exact calculations in this paper neglect the details of the spray roots. As will be seen in section 4.3, this can lead to an under-prediction of the impact force.

In this paper, we will first give the mathematical formulation followed by numerical techniques and convergence tests. Numerical results for various body shapes are given. It will be shown that the time-domain results agree with linear frequency-domain results for small amplitude motions. Nonlinear hydrodynamic forces are found for large-amplitude motions. Impact forces are examined for a wedge entering the water at high velocity and compared with other results. The problem of a body exiting from the water is also investigated. Contrary to linear theory, the hydrodynamic forces for the water entry problem are found to be significantly different from those for the water exit problem.

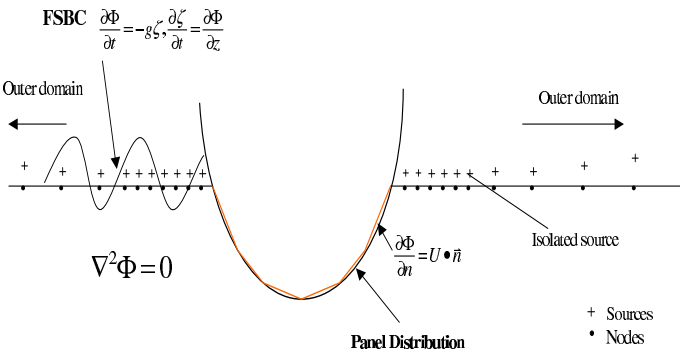

Figure 1: Definition Sketch

2 Mathematical formulation

We consider a general two-dimensional body floating on a free surface and undergoing arbitrary three-degree-of-freedom motions. An earth-fixed Cartesian coordinate system is chosen with the y-axis coincident with the quiescent free surface, and z-axis is positive upward. The fluid is assumed to be homogeneous, incompressible, inviscid and its motion is irrotational. Surface tension is neglected and the water depth is infinite. The fluid motions can be described by a velocity potential $\Phi(y,z,t)$. In the fluid domain, Φ satisfies the Laplace equation

$$\nabla^2\Phi = 0 \tag{1}$$

On the mean free surface, the linearized free surface boundary conditions are imposed

$$\zeta_t - \Phi_z = 0 \qquad \text{on} \quad z=0 \tag{2}$$

$$\Phi_t + g\zeta = 0 \qquad \text{on} \quad z=0 \tag{3}$$

where $z=\zeta(y,t)$ is the free surface amplitude, and g is the acceleration due to gravity. On the *instantaneous* body boundary, no normal flux is permitted

$$\frac{\partial\Phi}{\partial n} = V_n \quad \text{on} \quad S_b \tag{4}$$

where the unit normal vector into the body $\mathbf{n}$ is positive out of the fluid. V_n is the instantaneous velocity in the normal direction including rotational effects. In the far field, the radiation boundary condition needs to be imposed that there are no incoming waves. The initial conditions at $t=0$ are

$$\Phi = \Phi_t = 0 \quad \text{in the fluid domain} \tag{5}$$

At each time step, a mixed boundary value problem must be solved; the potential is given on the free surface and the normal derivative of the potential is known on the body surface. In terms of the desingularized sources above the calm water surface and sources distributed on the body surface, the potential at any point in the fluid domain can be given by

$$\Phi(\mathbf{x}) = \sum_{i=1}^{n} \sigma(\boldsymbol{\xi}_i)\ln|\mathbf{x}-\boldsymbol{\xi}_i| + \int_{S_w} \sigma(\boldsymbol{\xi})G(\mathbf{x};\boldsymbol{\xi})dl \tag{6}$$

where S_w represents the instantaneous wetted body surface. $|\mathbf{x}-\boldsymbol{\xi}_i|$ represents the distance between any point in the fluid domain and the desingularized source point. $G(\mathbf{x};\boldsymbol{\xi})$ is a Rankine source Green function

$$G(\mathbf{x};\boldsymbol{\xi}) = \ln r \tag{7}$$

$$r^2 = (y-\xi)^2 + (z-\eta)^2 \tag{8}$$

where r is the distance between a source point and a point in the fluid; $\boldsymbol{\xi}$ is the source point on the body boundary. Applying the boundary conditions, the integral equations that must be solved to determine the unknown source strengths are

$$\sum_{i=1}^{n} \sigma(\boldsymbol{\xi}_i) \ln|\mathbf{x}_c - \boldsymbol{\xi}_i| + \int_{S_w} \sigma(\boldsymbol{\xi}) G(\mathbf{x}_c, \boldsymbol{\xi}) dl = \Phi(\mathbf{x}_c) \quad \mathbf{x}_c \in \Gamma_d \tag{9}$$

$$\sum_{i=1}^{n} \sigma(\boldsymbol{\xi}_i) \frac{\partial \ln|\mathbf{x}_c - \boldsymbol{\xi}_i|}{\partial n} + \int_{S_w} \sigma(\boldsymbol{\xi}) \frac{\partial G(\mathbf{x}_c, \boldsymbol{\xi})}{\partial n} dl = \chi(\mathbf{x}_c) \quad \mathbf{x}_c \in \Gamma_n \tag{10}$$

Where $\boldsymbol{\xi}$ = a source point
$\mathbf{x}_c$ = a point on the real boundary
χ = the given normal velocity on the body boundary
Φ = the given potential on the free surface $(z = 0)$
Γ_d = the free surface
Γ_n = exact submerged body surface

Once the source strengthes are found, Φ can be evaluated by (6), and the velocity on the body $\nabla\Phi$ can be obtained. The total pressure is given by Bernoulli's equation

$$\begin{aligned} p &= -\rho\left(\frac{\partial \Phi}{\partial t} + \frac{1}{2}|\nabla\Phi|^2 + gz\right) \\ &= -\rho\left(\frac{\delta \Phi}{\delta t} - V \cdot \nabla\Phi + \frac{1}{2}|\nabla\Phi|^2 + gz\right) \end{aligned} \tag{11}$$

Where $\frac{\delta\Phi}{\delta t}$ is the change in Φ on a given node at each time step. V is the moving 'node' velocity due to repanelization. The forces acting on the body can be obtained by integrating (11) over the instantaneous submerged body surface, which can be written as

$$\mathbf{F} = \int_{S_w} p\mathbf{n}\, dl \tag{12}$$

3 Numerical method

In the usual manner, the integrals shown in equations (9) and (10) may be discretized to form a system of linear equations to be solved at each time step. As shown in Figure 1, on the desingularized boundary, the sources are distribution outside the domain so that the source points never coincide with the collocation or node points and the integrals are nonsingular. In addition, because of desingularization, isolated sources are used rather than a source distribution. This greatly reduces the computation complexity of the influence matrix. The isolated sources are distributed a small distance above the calm water surface. The nondimensional desingularized distance is given by

$$L_d = D_m^{0.5} \tag{13}$$

where D_m is the measure of the local mesh size, L_d is the desingularized distance [14]. In order to resolve the leading order radiated waves and minimize any wave reflection from the outer boundary, an inner and outer region is introduced in accord with the work of Lee [14]. The inner domain spans eight wavelengths, with the body in the center. The wavelength is determined by the wave dispersion relation $\lambda = \frac{2\pi g}{\omega^2}$. Here ω is the oscillation frequency of the body. To properly resolve the radiated waves, 30 nodes per wave length are uniformly distributed over the inner domain. Near the intersection between the free surface and body, special care needs to be taken to match the size of the panels on the free surface and the body surface.

In order to prevent wave reflection and maintain continuity, numerical beaches are placed near the truncation boundaries. An additional 20 nodes are spread out over 80 wavelengthes beyond the inner domain. The spacing of these nodes increases exponentially from the constant spacing of the inner domain to the end of the outer domain. The spacing, in equation (14) was determined by Lee [14] to minimize the wave reflections.

$$dx_{out_i} = dx_{in} \times 1.0378^{\frac{i(i-1)}{2}}, \qquad i = 1..20 \tag{14}$$

On the other hand, panels are distributed on the body surface, which are more suitable for any arbitrary body shape than the desingularized sources. The integral equations (9) and (10) are satisfied at the nodes on the free surface and body surface such that

$$\sum_{j=1}^{N_F} \sigma_j^F \ln|\mathbf{x}_{c_i}^F - \boldsymbol{\xi}_{s_j}^F| + \sum_{j=1}^{N_B} \sigma_j^B \int_{\Delta S_j} \ln|\mathbf{x}_{c_i}^F - \boldsymbol{\xi}_j^B| dl = \Phi(\mathbf{x}_{c_i}^F) \tag{15}$$

$$-\pi\sigma(\mathbf{x}_{c_i}^B) + \sum_{j=1}^{N_F} \frac{\sigma_j^F}{|\mathbf{x}_{c_i}^B - \boldsymbol{\xi}_{s_j}^F|} + \sum_{j=1, j\neq i}^{N_B} \sigma_j^B \int_{\Delta S_j} \frac{1}{|\mathbf{x}_{c_i}^B - \boldsymbol{\xi}_j^B|} dl = \chi(\mathbf{x}_{c_i}^B) \tag{16}$$

Where ΔS_j is the jth panel on the body surface. Equations (15) and (16) can be solved either by a direct or an iterative method depending on the size of the matrix. The LU decomposition method is used for calculations in this paper. Once the source strengthes are determined by solving the above equations, the fluid velocity on the free surface can be computed. Then the free surface elevation and the potential are updated by using the free surface boundary conditions (2) and (3). The time stepping is accomplished using a 2nd-order Adams-Bashforth scheme as in equations (17) and (18). The updated free surface locations and potentials are then used to start the mixed boundary value problem at the next time step and the evolution continues.

$$\zeta(t+\triangle t) = \zeta(t) + \frac{\triangle t}{2}[3(\frac{\partial\zeta}{\partial t})_t - (\frac{\partial\zeta}{\partial t})_{t-\triangle t}] \tag{17}$$

$$\Phi(t+\triangle t) = \Phi(t) + \frac{\triangle t}{2}[3(\frac{\partial\Phi}{\partial t})_t - (\frac{\partial\Phi}{\partial t})_{t-\triangle t}] \tag{18}$$

In order to ensure consistent free surface resolution over time for the body exact problem, the free surface nodes are relocated to a distribution consistent with the original distribution relative to the current displaced body. This is accomplished by interpolating both ζ and Φ by a cubic spline for the newly distributed nodes.

The force acting on the body is evaluated by integrating the pressure over the instantaneous submerged surface using equation (11). The $\partial\Phi/\partial t$ on the body is evaluated by

$$(\frac{\partial\Phi}{\partial t})_i^n = \frac{\delta\Phi_i}{\delta t} - V_i^n \cdot \nabla\Phi_i^n = \frac{\Phi_i^n - \Phi_i^{n-1}}{\Delta t} - V_i^n \cdot \nabla\Phi_i^n \tag{19}$$

where Φ_i^n is the velocity potential of ith node at the nth time step on the body. V_i^n is the moving velocity of the grid points due to the repanelization on the body surface at each time step. When the panel number changes between time steps for extremely large motion amplitudes, equation (19) can not be used directly. Before the the $(j+1)th$ time step when the panel number changes, the potential on the body nodes at the jth time step should be calculated again with the same panel number as at the $(j+1)th$ time step. The recalculated potential will be used to calculate the pressure at the $(j+1)th$ time step by using equation (19).

4 Results

4.1 Linear radiation problem

To verify the method, forced small amplitude motions of a circular cylinder of radius R and a box ($B/T = 2.0$) are calculated including heave, sway, and roll motions. The body boundary condition is satisfied at the mean body position. The area of cylinder section is A. The motion amplitude of the circular cylinder in heave and sway is $a = 0.1R$. The motion amplitude of the box in heave and sway is $a = 0.1T$. The motion amplitude of the box in roll is $a = 0.1\pi$. Once the force time histories are calculated, the added mass and damping coefficients can be obtained by using Fourier analysis. The calculated added mass and damping coefficients are compared with the experimental results of Vugts [15] and the results computed using a free surface Green function (see for example Frank [2]).

Figure 2 shows the convergence of the added mass of a circular cylinder both for the time step number in one time period and panel number on the body surface. The convergence curves suggest the good convergence characteristics of this method. The panel number is $N = 40$ on the body surface, and the time step size $\triangle t$ is $T_{period}/100$. Figure 3 and Figure 4 show the added mass and damping of the circular cylinder. Figure 5, Figure 6 and Figure 7 show the added mass and damping of a box in heave, sway, and roll respectively. The comparisons shown in these figures are satisfactory and verify the accuracy of the present method for the linear problem.

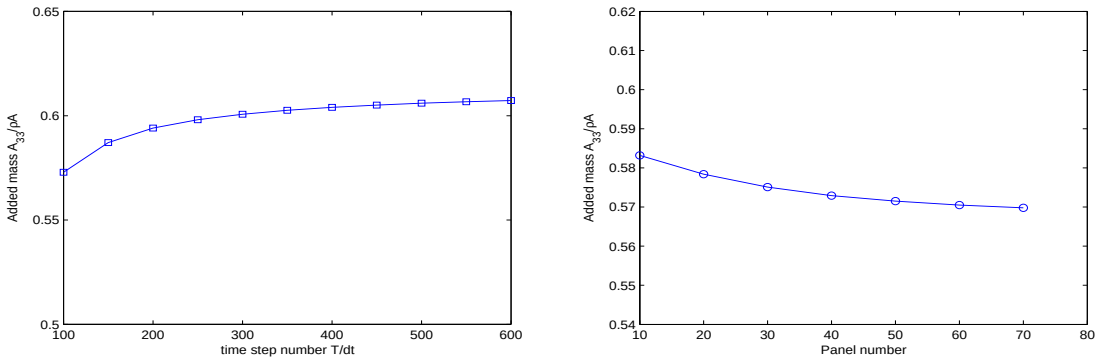

Figure 2: Convergence of added mass of a circular cylinder in heave motion, $a = 0.1R$

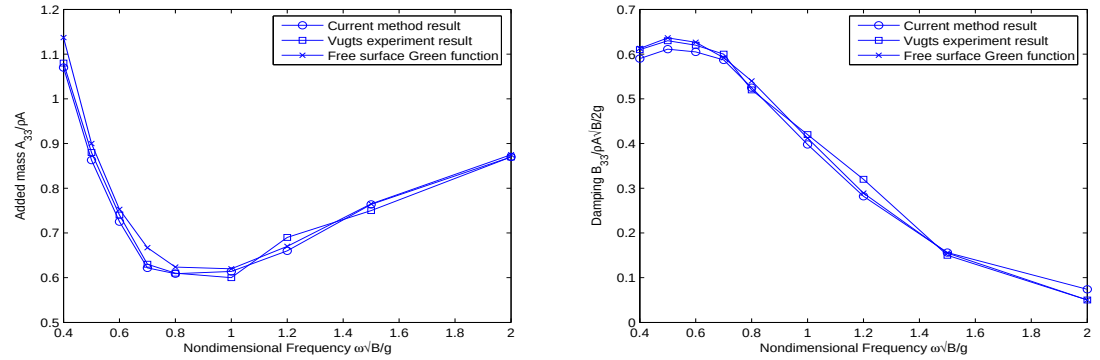

Figure 3: Added mass and damping coefficients of circular cylinder in heave motion

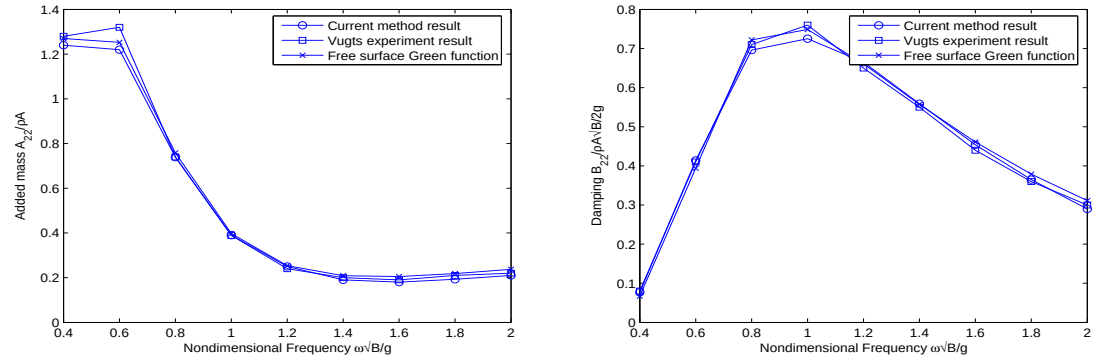

Figure 4: Added mass and damping coefficients of circular cylinder in sway motion

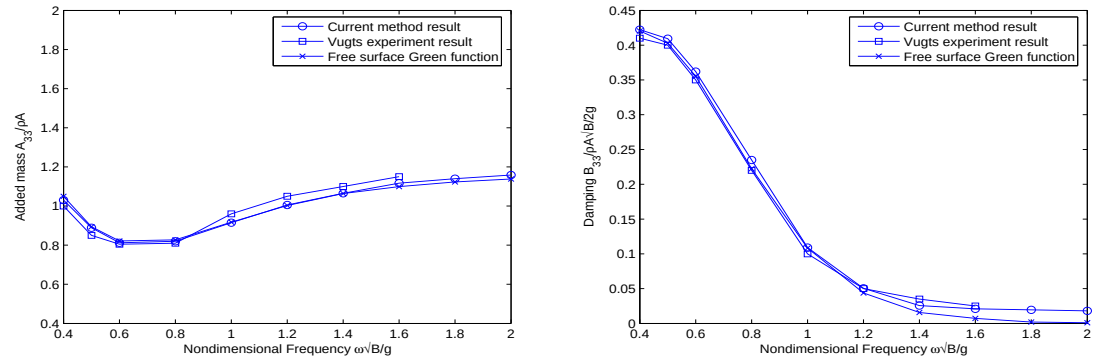

Figure 5: Added mass and damping coefficients of a box in heave motion

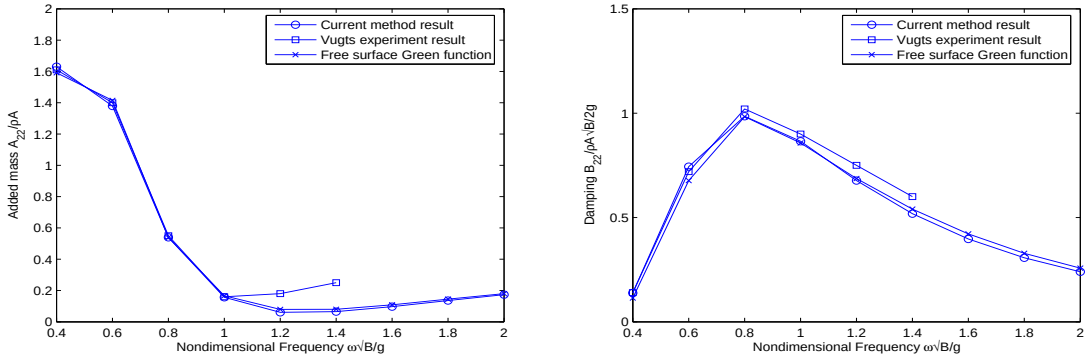

Figure 6: Added mass and damping coefficients of a box in sway motion

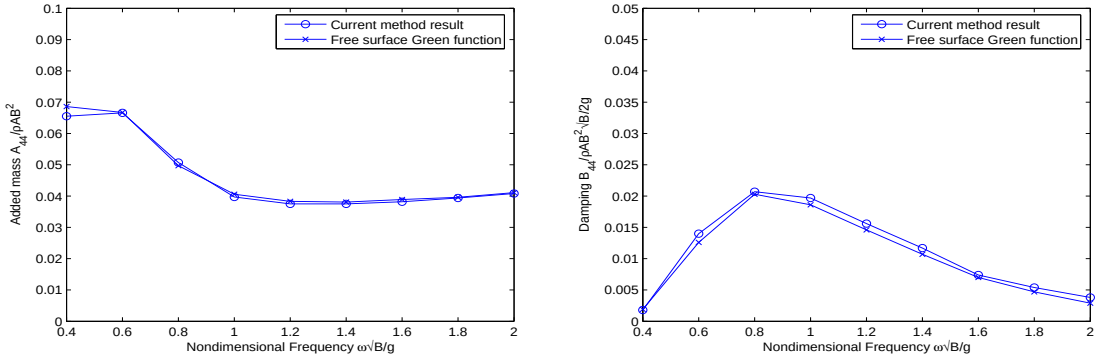

Figure 7: Added mass and damping coefficients of a box in roll motion

4.2 Body-exact problem

As an example, the forced large amplitude motion of a circular cylinder of radius R is studied here. The cylinder is initially submerged such that the center is at the calm water line. The forced heave motion is $z(t) = -a\sin\omega t$, where a is the motion amplitude. We set $\frac{\omega R}{g} = 1.0$. Again, the panel number is $N = 40$ on the submerged body surface, and the time step size $\triangle t$ is $T_{period}/100$. As addressed earlier, at each time step, the submerged portion of the cylinder is repanelized, and the influence matrix is reevaluated.

Figure 8 shows the different components of the vertical force acting on the circular cylinder for the case of $a/R = 0.5$. The steady state is rapidly reached. As shown, the hydrostatic force is the largest part of the force. The inertia term $\partial\Phi/\partial t$ shows a higher-harmonic component. The quadratic component $(-|\nabla\Phi|^2/2)$ is primarily a second-order harmonic. It's magnitude is very close to the moving grid term.

The frequency components of the total force can be obtained by using Fourier analysis. The force coefficients are nondimensionlized according to Yamashita [16]

$$F_0^2 = \frac{|F(0)| - \rho g A_s}{2\rho g A^2} \tag{20}$$

$$F_a^1 = \frac{|F(\omega)|}{2\rho g R A} \tag{21}$$

$$F_a^2 = \frac{|F(2\omega)|}{2\rho g A^2} \tag{22}$$

where $|F(\omega)|$ is the amplitude of the Fourier component of the force at that frequency and is determined using a Fourier transform. A_s is the mean submerged cross section area. F_0^2 is the second-order mean force; F_a^1 is the first-order harmonic force; F_a^2 is the second-order harmonic force.

For $a/R = 0.2$, the frequency components of the vertical force are given in normalized form in the Table 1. The values are compared with the experiments of Yamashita [16] and numerical results of Kent [17] obtained by using a 3rd-order pseudo-spectral method. The comparisons in Table 1 show good agreement for the mean force and the first-order force. Present calculations also capture the main part of second order force. The agreement is surprisingly good considering only a linearized free surface boundary condition is used. It

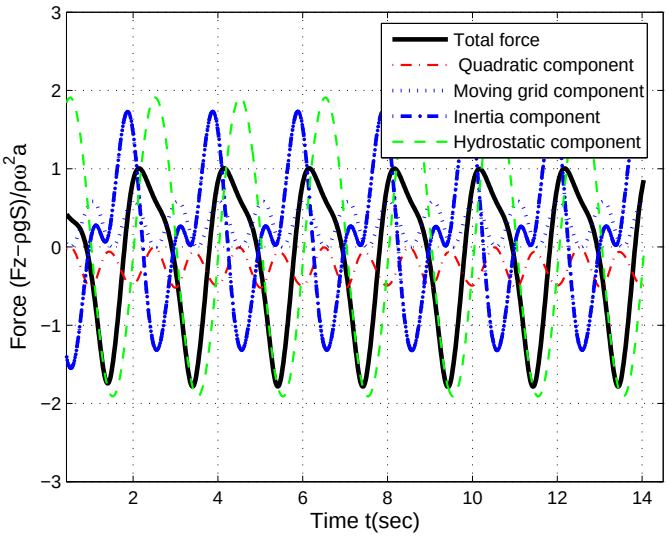

Figure 8: Vertical force acting in the circular with $a = 0.5R$, $\omega^2 g/R = 1.0$

a/R=0.2	$\frac{\omega^2 R}{g}$	F_0	F_1	a_{33}	b_{33}	F_2
Yamashita (1977)	0.5	-0.01	/	0.66	0.72	0.15
Kent (2005)	0.5	-0.01	0.821	0.60	0.796	0.194
Present calculation	0.5	-0.013	0.815	0.61	0.62	0.163
Yamashita (1977)	1.0	-0.08	/	0.60	0.39	0.45
Kent (2005)	1.0	-0.086	0.615	0.58	0.375	0.491
Present calculation	1.0	-0.097	0.632	0.59	0.41	0.428
Yamashita (1977)	1.5	-0.15	/	0.69	0.22	0.8
Kent (2005)	1.5	-0.16	0.36	0.62	0.209	0.796
Present calculation	1.5	-0.20	0.378	0.65	0.28	0.62

Table 1: Comparing frequency component amplitudes of the vertical force on circular for large amplitude motion

also suggests that in this case, the nonlinear effects associated with the geometry play a more important role than the wave nonlinearities.

4.3 Water entry and exit problem

The impact problem for 30, 45, and 60 degree wedges was investigated. The pressures over the wedges and slamming forces were compared with the similarity solutions presented by Zhao and Faltinsen [13]. The initial conditions were set such that wedges had negligible initial draft and a constant downward velocity of 10 meters-per-second. The pressure values are only plotted once the solution reaches a relatively steady state. The relative steady state can be seen in Figure 12. As can be seen, the slamming force reaches an almost constant value after the initial large impact force that occurs as the body initially enters the water. The pressure distributions on the wedges during impact are shown in Figure 9, Figure 10, and Figure 11 for wedges of 30, 45, and 60 degrees respectively. As can be seen, there is significantly disagreement between the similarity solution of Zhao and Faltinsen [13] and the pressure distribution to $z = 0$. It is proposed to improve the solution by 'stretching'. Using equation (3), the intersection of the free surface and the wedge can be calculated. Once the wetted surface is known, the pressure distribution can be stretched up to that point. The stretched pressure distributions are also shown in Figure 9, Figure 10, and Figure 11. The agreement with the similarity solution is greatly improved. Figure 12 shows the impact force acting on a 45-degree wedge found by integrating the pressures. All these values are compared with the similarity solution. As can be seen, the unstretched values in these figures are the smallest, which are very close to the Von Karman's solution, nearly half of the similarity solution. The comparisons also suggest that impact pressures and forces calculated using the stretching technique are much better than the unstretched results. While the agreement is not perfect, the results do show that this computationally fast, simplified model gives reasonable results.

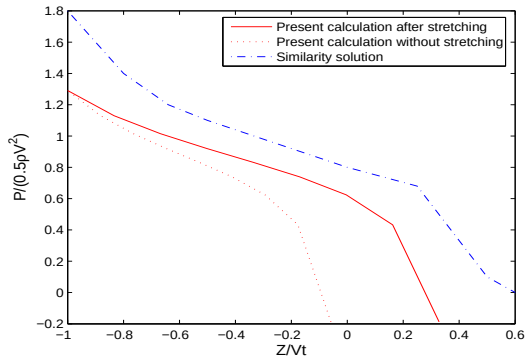

Figure 9: Pressure distribution over a 30-degree wedge

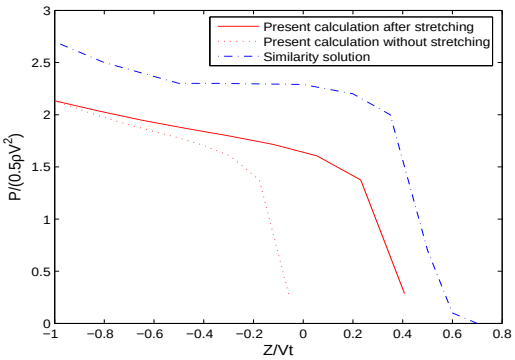

Figure 10: Pressure distribution over a 45-degree wedge

Figure 13 and Figure 14 show the force time history acting on a 45-degree wedge undergoing large amplitude sinusoidal motion. The body enters the water at $t = 0$ sec, and reaches the bottom of the down stroke at $t = 0.5$ sec. At $t = 1$ sec the body exits the water and remains out of the water until it reenters at $t = 2$ sec. The cycle then repeats itself. Figure 13 shows the force time history for a $\Phi = 0$ free surface boundary condition. This is the free surface boundary condition normally used for the impact problem. The dashed curve shows the displacement of the wedge as a function of time. As can be seen, the exit force and entry force are identical. Figure 14 shows the force time history due to the same displacement time history as in Figure 13, but using the linearized free surface boundary conditions. On the water entering phase of the motion, the stretching technique is applied. As the wedge starts to exit the water the computed wave amplitude near the body reverses and becomes negative. The negative wave amplitude may become larger than the body draft. Consequently, the stretching is turned off as soon as the predicted wave amplitude near the body becomes negative. As shown in Figure 14, for small times, the impact force is consistent with the water entry problem. In addition, the shape of the entry force curve in Figure 14 has the same form as in Figure 13. However, the water exit force curve in Figure 14 shows a significant difference from the exit force curve in the $\Phi = 0$ problem (Figure 13). The differences are due to the free surface boundary conditions and the formation of free surface waves.

5 Conclusions

Two-dimensional, large amplitude body motion is studied in this paper with a linearized free surface and exact body boundary conditions. Numerical results are obtained for small amplitude motion, large amplitude motion, water entry and water exit. Convergence and accuracy are verified for small amplitude motions. Compared with the experiments and other numerical solutions, good agreement was found for the large amplitude oscillation problem of a circular cylinder. For the wedge impact problem, the calculated values are smaller than the similarity solutions due to the lack of spray roots. The results of the water exit problem demonstrate that the memory effects of the free surface are important.

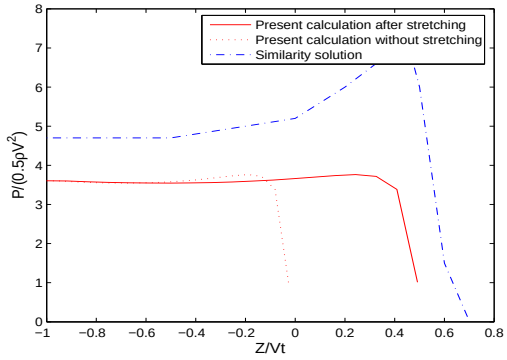

Figure 11: Pressure distribution over a 60-degree wedge

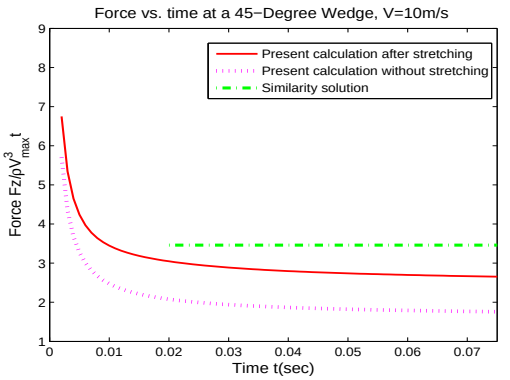

Figure 12: Impact force acting on a 45-degree wedge

6 Acknowledgement

The authors would like to express their appreciation to Prof. Troesch of the Naval Architecture and Marine Engineering Department for discussions regarding the this work. This work was supported by Office of Naval Research, contracts N00014-04-1-0266 and N00014-05-1-0537.

References

[1] N. Salvesen, E. O. Tuck, and O. Faltinsen, Ship motions and sea loads. *Trans. SNAME*, Vol. 78 (1970) pp. 250-287

[2] W. Frank, On the oscillation of cylinders in or below the free surface of deep fluids. *Naval Ship Research and Development Center Report*, No. 2375 (1967)

[3] C.-H. Lee and J. N. Newman, Computation of wave effects using the panel method. *Numerical models in fluid-structure interaction*, Editor S. Chakrabarti, WIT Press, Southhampton (2004)

[4] R. F. Beck and A. M. Reed, Modern seakeeping computations for ships in seaway. *SNAME Transactions 109* (2001) pp. 1-52

[5] M. S. Longuet-Higgins and E. D. Cokelet, The deformation of steep surface waves on water: I. A numerical method of computation. *Proc. Roy. Soc. Lond.*, Ser. A, A 350 (1976) pp. 1-26

[6] R. F. Beck, Fully nonlinear water wave computations using a desingularized Euler-Lagrange time-domain approach. *Nonlinear Water Wave Interaction*, WIT Press (1999) pp. 1-58

[7] P. D. Sclavounos, Computations of wave ship interactions. *Advances in Marine Hydrodyanmics*, Editor, M. Ohkusu, Computational Mechanics Publications (1996) pp. 233-278

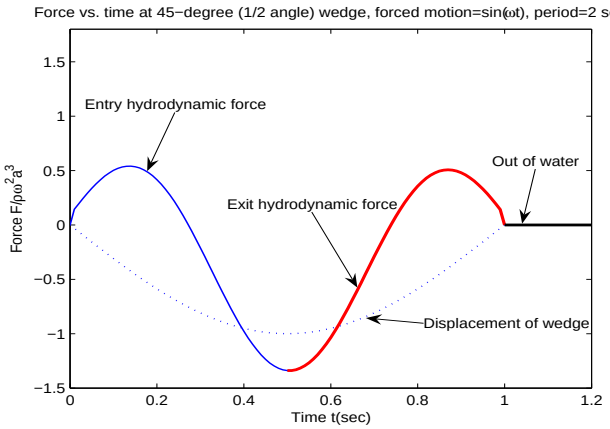

Figure 13: Force acting on a 45-degree wedge in large amplitude sinusoidal motion with $\Phi = 0$ at the free surface

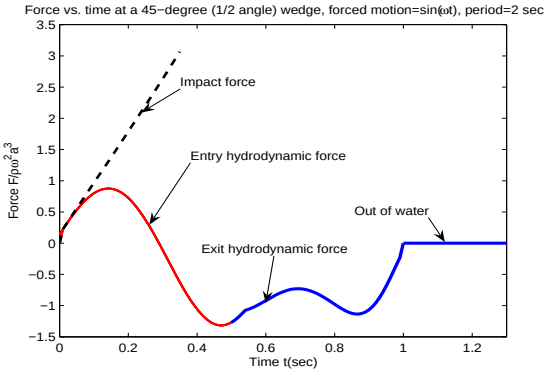

Figure 14: Force acting on a 45-degree wedge in large amplitude sinusoidal motion with linearized free surface boundary conditions

[8] J. Jensen, R. F. Beck, S. Du, O. Faltinsen, N. Fonseca, E. Rizzuto, D. Stredulinsky, and I. Watanabe, Extreme Hull Girder Loading. *Proceedings 14th International Ship and Offshore Structures Congress*, Nagasaki, Japan, Vol. 2 (2000) pp. 236-320

[9] P. Finn, R. F. Beck, A. W. Troesch, and Y. S. Shin, Nonlinear impact loading in an oblique seaway. *Journal of Offshore Mechanics and Arctic Engineering*, Vol. 125, No. 3 (2002) pp. 190-197

[10] T. Von Karman, The impact on seaplane floats during landing. *NACA TN 321* (1929)

[11] H. Wagner, Über stoss- und gleitvergänge an der oberfläche von flüssigkeiten. *ZAMM*, Vol. 12 (1932) pp. 193-215

[12] Z. N. Dobrovol'skaya, On some problems of similarity flow of fluid with a free surface. *J. Fluid Mech.*, Vol. 36, part4, (1969) pp. 805-829

[13] R. Zhao, O. Faltinsen, Water entry of two-dimensional bodies. *J. Fluid Mech.*, Vol. 246 (1993) pp. 593-612

[14] T. -H. Lee, Nonlinear radiation problems for a surface-piercing body. PhD. Thesis, Department of Naval Architecture and Marine Engineering, The University of Michigan, USA (1992)

[15] J. H. Vugts, The hydrodynamic coefficients for swaying, heaving and rolling cylinders on a free surface. Shipbuilding Laboratory, Technical University Delft, Report No. 112 S (1968)

[16] S. Yamashita, Calculation of hydrodynamic forces acting upon thin cylinders oscillating vertically with large amplitude. *J. Soc. Nav. Arch.* No. 141 Japan (1977) pp. 61-70

[17] C. P. Kent, A pseudo-spectral method for calculating wave-body interaction using an explicit free-surface formulation. PhD. Thesis, Department of Naval Architecture and Marine Engineering, The University of Michigan (2005)